Virology 468-470 (2014) 36–46

Contents lists available at ScienceDirect

Virology

journal homepage: www.elsevier.com/locate/yviro

The Cucumber leaf spot virus p25 auxiliary replicase protein binds and modifies the endoplasmic reticulum via N-terminal transmembrane domains

Kankana Ghoshal [a], Jane Theilmann [b], Ron Reade [b], Helene Sanfacon [b], D'Ann Rochon [a,b,*]

[a] University of British Columbia, Faculty of Land and Food Systems, Vancouver, British Columbia, Canada V6T 1Z4
[b] Agriculture and Agri-Food Canada Pacific Agri-Food Research Centre, 4200 Hwy 97, Summerland, British Columbia, Canada V0H 1Z0

ARTICLE INFO

Article history:
Received 10 June 2014
Returned to author for revisions
28 June 2014
Accepted 13 July 2014
Available online 16 August 2014

Keywords:
Aureusvirus
Auxiliary replicase
Endoplasmic reticulum
Tombusviridae

ABSTRACT

Cucumber leaf spot virus (CLSV) is a member of the *Aureusvirus* genus, family *Tombusviridae*. The auxiliary replicase of Tombusvirids has been found to localize to endoplasmic reticulum (ER), peroxisomes or mitochondria; however, localization of the auxiliary replicase of aureusviruses has not been determined. We have found that the auxiliary replicase of CLSV (p25) fused to GFP colocalizes with ER and that three predicted transmembrane domains (TMDs) at the N-terminus of p25 are sufficient for targeting, although the second and third TMDs play the most prominent roles. Confocal analysis of CLSV infected 16C plants shows that the ER becomes modified including the formation of punctae at connections between ER tubules and in association with the nucleus. Ultrastructural analysis shows that the cytoplasm contains numerous vesicles which are also found between the perinuclear ER and nuclear membrane. It is proposed that these vesicles correspond to modified ER used as sites for CLSV replication.

Introduction

Virus replication requires host membranes and is known to induce membrane and organelle alterations during infection (Ahlquist et al., 2003; den Boon et al., 2010; Laliberte and Sanfacon, 2010; Miller and Krijnse-Locker, 2008; Rochon et al., 2014). Such changes include the formation of vesicles, multivesicular bodies such as those associated with peroxisomes or mitochondria in tombusvirus infections (McCartney et al., 2005; Panavas et al., 2005; Rochon et al., 2014; Rubino et al., 2001) and spherules which are associated with numerous RNA viruses (Ahlquist et al., 2003; den Boon et al., 2010; Laliberte and Sanfacon, 2010; Rochon et al., 2014). In the case of *Brome mosaic virus* (BMV) infection, the auxiliary replicase 1a protein contributes to the formation of spherules (Schwartz et al., 2002, 2004). In several viruses, specific transmembrane domains anchor the replicase or replication associated protein to membranes. This includes the BMV 1a protein (den Boon et al., 2010; Liu et al., 2009), the *Tobacco mosaic virus* 126K protein (dos Reis Figueira et al., 2002), the *Red clover necrotic mosaic virus* (RCNMV) p27 protein (Kusumanegara et al., 2012; Turner et al., 2004), the tombusvirus p33/p36 protein (Hwang et al., 2008; McCartney et al., 2005; Navarro et al., 2004; Panavas et al., 2005), the *Tobacco etch virus* (TEV) 6K2 (Schaad et al., 1997), the *Tomato ringspot virus* (ToRSV) NTB-VPg and X2 proteins (Zhang and Sanfacon, 2006; Zhang et al., 2005), the *Flock house virus* (FHV) protein A (Van Wynsberghe et al., 2007) and the *Poliovirus* 2C and 3AB proteins (Echeverri and Dasgupta, 1995; Teterina et al., 1997; Towner et al., 1996).

Cucumber leaf spot virus (CLSV) is a member of the *Aureusvirus* genus in the family *Tombusviridae* and is most closely related to the *Tombusviruses* (Rochon et al., 2012). The approximate 4.4 kb single-stranded positive sense RNA genome contains 5 open reading frames (ORFs) (Fig. 1). ORF1 encodes an essential 25 kDa protein (p25) that shows sequence similarity with the p33 auxiliary replicase protein of tombusviruses as well as the analogous protein of other members of the *Tombusviridae* (Rochon et al., 2012). Readthrough of ORF1 produces an 84 kDa protein that contains the RNA dependent RNA polymerase motifs. ORF3 encodes the 41 kDa coat protein (CP) that assembles with viral RNA to form virions with $T=3$ icosahedral symmetry. p27 is translated from ORF4 and has been shown to be required for cell-to-cell movement. p17, translated from ORF5, has been shown to be involved in symptom induction and is likely a suppressor of RNA silencing as it shows sequence similarity to the silencing suppressors of tombusviruses (Rochon et al., 2012). p25 and p84 are translated directly from genomic RNA while the CP is

* Corresponding author at: Agriculture and Agri-Food Canada Pacific Agri-Food Research Centre, 4200 Hwy 97, Summerland, British Columbia, Canada V0H 1Z0. Tel.: +1 250 494 6394; fax: +1 250 494 0755.
E-mail address: dann.rochon@agr.gc.ca (D. Rochon).

http://dx.doi.org/10.1016/j.virol.2014.07.020
0042-6822/

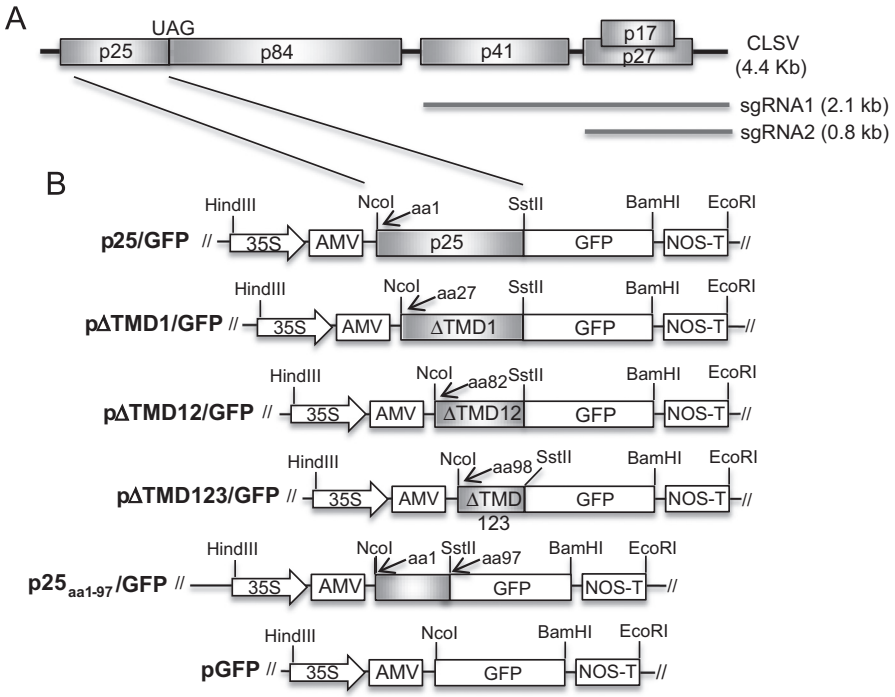

Fig. 1. Structure of the CLSV genome and of p25 mutant constructs used for agroinfiltration. A) The genomic location of the 5 proteins encoded by the CLSV genome (see text for further details). B) Deletion mutant constructs of p25 used for agroinfiltration were cloned into the binary vector pBINPLUS which contains the *Cauliflower mosaic virus* 35S promoter, the *Alfalfa mosaic virus* (AMV) translational enhancer and the nopaline synthase transcription terminator. The N-terminal aa is shown for each N-terminal deletion mutant, i.e., pΔTMD1/GFP, pΔTMD12/GFP and pΔTMD123/GFP, which lack either the N-terminal 26, 81 or 96 aa respectively of p25. $p25_{aa1-97}$/GFP contains the N-terminal 97 aa of p25, whereas the remaining sequence is deleted.

translated from a 2.1 kb subgenomic RNA1 (sgRNA1). p27 and p17 are translated from distinct overlapping ORFs on the 0.8 kb sgRNA2 (Fig. 1) (Miller et al., 1997; Reade et al., 2003).

The site of replication of aureusviruses is currently unknown. Other tombusvirids are known to replicate in association with peroxisomes, as is the case for the tombusviruses *Tomato bushy stunt virus* (TBSV), *Cymbidium ringspot virus* and *Cucumber necrosis virus* (CNV) (McCartney et al., 2005; Navarro et al., 2004; Panavas et al., 2005; Rochon et al., 2014), mitochondria in the case of another tombusvirus *Carnation Italian ringspot virus* (CIRV) (Hwang et al., 2008; Rubino et al., 2001) and the carmovirus *Melon necrotic spot virus* (MNSV) (Mochizuki et al., 2009) and the endoplasmic reticulum (ER) in the case of the dianthovirus RCNMV (Kusumanegara et al., 2012; Turner et al., 2004). In the tombusviruses, the auxiliary replicase protein, p33, contains the determinants for peroxisomal or mitochondrial targeting (Hwang et al., 2008; McCartney et al., 2005; Navarro et al., 2004; Panavas et al., 2005; Rubino et al., 2001). Similarly, the auxiliary replicase proteins of MNSV and RCNMV contain specific domains essential for association with either the mitochondria or ER, respectively (Kusumanegara et al., 2012; Mochizuki et al., 2009; Turner et al., 2004). Viruses of other families are also known to replicate in association with specific membranes including the ER for BMV (den Boon et al., 2001; Liu et al., 2009), ToRSV (Zhang et al., 2005; Zhang and Sanfacon, 2006), Poliovirus (Echeverri and Dasgupta, 1995; Teterina et al., 1997; Towner et al., 1996) and Hepatitis C virus (Brass et al., 2002; Schmidt-Mende et al., 2001) the chloroplast for the tymovirus *Turnip yellow mosaic virus* (Prod'homme et al., 2003) and mitochondria for FHV (Miller et al., 2001; Van Wynsberghe et al., 2007).

As stated above, the site of replication of the aureusvirus, CLSV, is not known. We provide evidence that a GFP fusion of CLSV p25, the auxiliary replicase protein, colocalizes with the ER. Aggregates of p25/GFP are also produced and may represent vesicles that are derived from the ER or aggregates of protein tethered to the ER. We have also identified 3 transmembrane domains (TMDs) at the N-terminus of p25 that are sufficient for targeting, and have found that the second and third TMDs play the most prominent roles. Consistent with these observations is our finding that CLSV infection alters ER structure including the formation of aggregates which are also associated with the nuclear ER. Ultrastructural analysis of CLSV infected plants shows that the cytoplasm contains numerous vesicles which may correspond to ER derived vesicles as deduced from the aggregates observed by confocal microscopy analysis. Similar vesicles are found in association with the nucleus. This is the first study to address the subcellular site of replication of an aureusvirus.

Results and discussion

Subcellular distribution of CLSV p25 fused to GFP in agroinfiltrated leaves of Nicotiana benthamiana

CLSV p25 was fused to the N-terminus of GFP in a binary vector (Fig. 1B) and used in agroinfiltration studies to address the subcellular location of p25. Localization of fused and unfused control GFP was analyzed in epidermal cells of *N. benthamiana* by confocal microscopy. In cells infiltrated with unfused GFP, fluorescence was found within the nucleus and in the cytoplasm along the cell periphery as expected (Fig. 2A, panel 1). In contrast p25/GFP localized to large amorphous aggregates (Fig. 2A, panel 2; see arrows) and to an ER-like network (Fig. 2A, panel 3). Nuclei were labeled along the periphery (Fig. 2A, panel 2; see closed arrowheads). Smaller sometimes mobile punctate structures along the periphery of the cells were also observed (Fig. 2A, panel 2, see open arrowhead). The identity of the mobile structures was not investigated but it is possible that they represent vesicles which during infection may serve to move viral RNA within the cell and to the plasmadesmata as has been described for other viruses

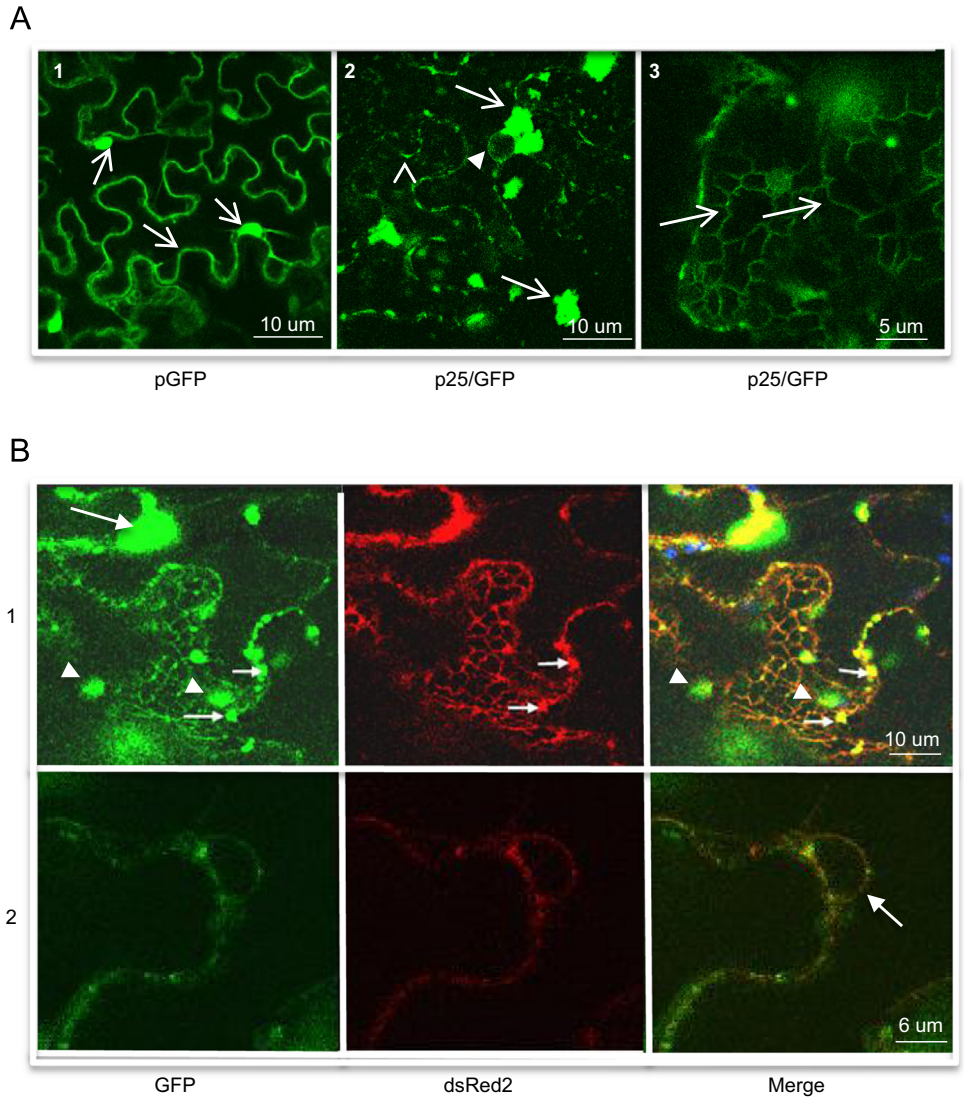

Fig. 2. Confocal microscopy of cells agroinfiltrated with p25/GFP. (A) Leaves of *N. benthamiana* were agroinfiltrated with CLSV p25/GFP and the subcellular sites of targeting were analyzed at 2–7 dpi using confocal microscopy. Panel 1 shows an epidermal cell from a leaf agroinfiltrated with unfused GFP. Note that the nucleus is filled and the periphery of the cell (cytoplasm) is labeled as expected. Panels 2 and 3 correspond to p25/GFP infiltrated epidermal cells. Notable features include large aggregates distributed throughout the cell but often in association with the nucleus (see arrows in panel 2), label in association with the periphery of the nucleus (see closed arrowhead, panel 2) and the presence of smaller aggregates or mobile foci along the periphery of the cell (see open arrowhead in panel 2). The higher magnification view in panel 3 shows that fluorescence is observed in association with a web-like structure reminiscent of the ER (arrows). (B) Construct p25/GFP colocalizes with pER-dsRed2, a construct that specifically targets the endoplasmic reticulum. Each agroinfiltration experiment (rows 1, 2) included p25/GFP, p19 and the pER-dsRed2 marker. The first column shows p25/GFP fluorescence and the second column shows pER-dsRed2 fluorescence. The third column (Merge) corresponds to the digitally superimposed images. Row 1 shows an epidermal cell in which the pER-dsRed2 signal appears as a network. It can be seen that the p25/GFP signal colocalizes with the ER marker. p25/GFP also produced punctae and large amorphous structures which may (arrows) or may not (arrowheads) have corresponding signals in the pER-dsRed2 image (see text). Row 2 shows colocalization of p25/GFP with pER-dsRed2 in a ring surrounding the nucleus (see arrow in merged image).

(Schoelz et al., 2011). However further research is required to demonstrate this possibility.

CLSV p25/GFP associates with the endoplasmic reticulum in agroinfiltrated N. benthamiana

The clear reticular pattern observed in cells of p25/GFP infiltrated leaves suggested that p25/GFP targets the ER. This was assessed by determining if p25/GFP colocalized with ER-specific dsRed2 (pER-dsRed2) that contains an ER targeting N-terminal signal peptide sequence along with an ER retention signal (HDEL) (Zhang et al., 2005). p25/GFP plus pER-dsRed2 coinfiltrated plants were examined by confocal microscopy. It can be seen in Fig. 2B (row 1) that the reticular pattern associated with p25/GFP expression in epidermal cells co-localized with the pER-dsRed2 fluorescence. In addition, some of the smaller green aggregates or punctae colocalized with pER-dsRed2 punctae. Similar punctae were not present in leaf tissue infiltrated with pER-dsRed2 alone (not shown) indicating that they represent local elaborations of the ER membrane induced by p25/GFP. These "aggregates" may correspond to vesicles that are derived from the ER as numerous vesicles can be found in CLSV infected leaf tissue as determined by ultrastructural analysis (see below). Larger green fluorescent aggregates in this image did not contain a corresponding red fluorescent signal (see arrowheads) suggesting that these correspond to primarily p25/GFP protein aggregates (which are later shown to be membrane anchored—see below). Fig. 2B (row 2) shows that CLSV p25/GFP also targets the perinuclear ER as indicated by its colocalization with pER-dsRed2 (see arrow in merged image).

CLSV infection induces a distinctive ER morphology in N. benthamiana 16c plants

Transgenic *N. benthamiana* 16c plants in which the ER is labeled with GFP were inoculated with CLSV to investigate whether infection induces morphological changes in the ER. At 2 days post-inoculation (dpi) confocal microscopy showed many punctae in the ER network at connections between tubules (Fig. 3, panel 2; see arrow). In addition, tubules were less defined or absent (see arrowhead). This is distinct from the typical reticular pattern observed in uninfected plants (Fig. 3, panel 1). Fig. 3 (panel 3) shows that the nucleus of CLSV infected plants is also distinct, i.e., numerous punctae or aggregates are present whereas in uninfected leaves the nucleus shows a smooth perinuclear ER boundary (Fig. 3, panel 1, see arrowhead). By 5 dpi, infected cells show a highly irregular pattern with many punctae and apparent aggregates of ER and little discernible ER network (Fig. 3, panel 4). As described above the aggregates may correspond to vesicles derived from the ER. Thus it is possible that targeting of CLSV p25 to the ER during infection results in a disordering of the ER network and elaborations of the ER (vesicles) that may serve as sites of viral RNA replication.

Deletion of two predicted transmembrane domains at the amino terminus of p25 results in partial loss of ER targeting of p25

In initial analyses, four protein transmembrane domain (TMD) prediction programs, HMMTOP, PHDhtm, TMHMM and TMpred (Hirokawa et al., 1998; Hofmann and Stoffel, 1993; Rost et al., 1996; Sonnhammer et al., 1998; Tusnady and Simon, 2001) were used to assess the possibility of transmembrane domain signals in p25 as a means to determine the manner in which p25 associates with the ER membrane. Fig. 4 shows that three of the programs (HMMTOP, TMHMM, TMpred) predict two major TMDs at the p25 N-terminus whereas a 4th (PHDhtm) predicts a single TMD. From the combined data, two transmembrane deletion mutant constructs of p25 fused to GFP were created. One, pΔTMD1/GFP (Fig. 1), contained a 26 amino acid N-terminal deletion of p25 to remove the first predicted transmembrane domain (Fig. 4) and the second, pΔTMD12/GFP (Fig. 1), contained an 81 aa N-terminal deletion to remove the first and second predicted transmembrane domains along with the intervening sequence between the two TMDs (Fig. 4). Confocal microscopy of plants co-infiltrated with either of these constructs and pER-dsRed2 was conducted to assess the role of one or both of the TMDs in targeting of p25 to the ER. Fig. 5A shows that pΔTMD1/GFP retains the ability to colocalize with pER-dsRed2. This suggests that TMD1 plays a minimal or no role in targeting. However, in the case of pΔTMD12/GFP the green fluorescence associated with the ER was less sharp than that of pΔTMD1/GFP (compare the GFP channel of Fig. 5A with that of Fig. 5B (row 1). More markedly, the ER of the corresponding dsRed image in Fig. 5B (row 1) is much sharper than that of the GFP image. Also, when mesophyll cells of pΔTMD12/GFP infiltrated plants were observed, although the ER was labeled, and again not sharply, green fluorescence was also found to occur in the cytoplasm (Fig. 5B, row 2, see closed arrowheads). Thus, the results

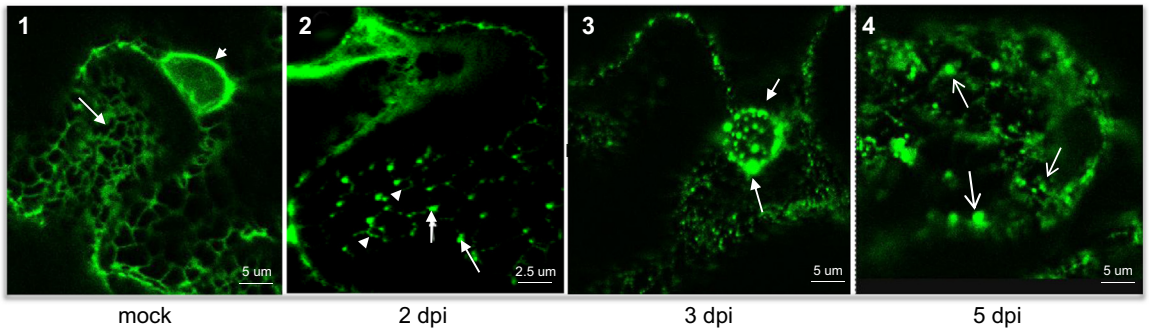

Fig. 3. CLSV infection results in remodelling of the endoplasmic reticulum. CLSV was inoculated onto transgenic *N. benthamiana* 16C plants that express an ER directed GFP fusion protein (kindly provided by D. Baulcombe). Plants were examined by confocal microscopy over a 5 days period. (1) Fluorescent ER structure of a mock inoculated cell showing the typical reticulate pattern and the perinuclear ER. The arrow points to an ER tubule and the arrowhead to the perinculear ER. (2) CLSV infected cells at 2 dpi showing partial disintegration of the ER network and the development of punctate foci along the ER network junctions (arrows). The arrowheads point to the barely visible ER tubules. (3) By 3 dpi the nucleus developed prominent punctate structures indicative of local elaborations of the nuclear ER or nuclear membrane (arrows). (4) CLSV infected cells at 5 dpi showing that the ER network appears to be largely disintegrated and punctae or larger aggregates of ER membrane are formed.

Fig. 4. Computer-assisted analysis of putative transmembrane helices in the N-terminal region of p25. Amino acid sequences of the N-terminal region of p25 are shown. Amino acid residues constituting the putative transmembrane domains of p25 predicted with the 5 indicated transmembrane helix prediction programs are colored red. The ΔTMD1/GFP N-terminal domain mutant begins at the valine (V) at aa position 27 and that of ΔTMD12/GFP begins at the threonine residue at position 82. ΔTMD123/GFP begins at the arginine residue at position 98. Thus in ΔTMD1/GFP, aa 2–26 of p25 are deleted, in ΔTMD12/GFP aa 2–81 of p25 are deleted and in ΔTMD123/GFP aa 2–97 are deleted.

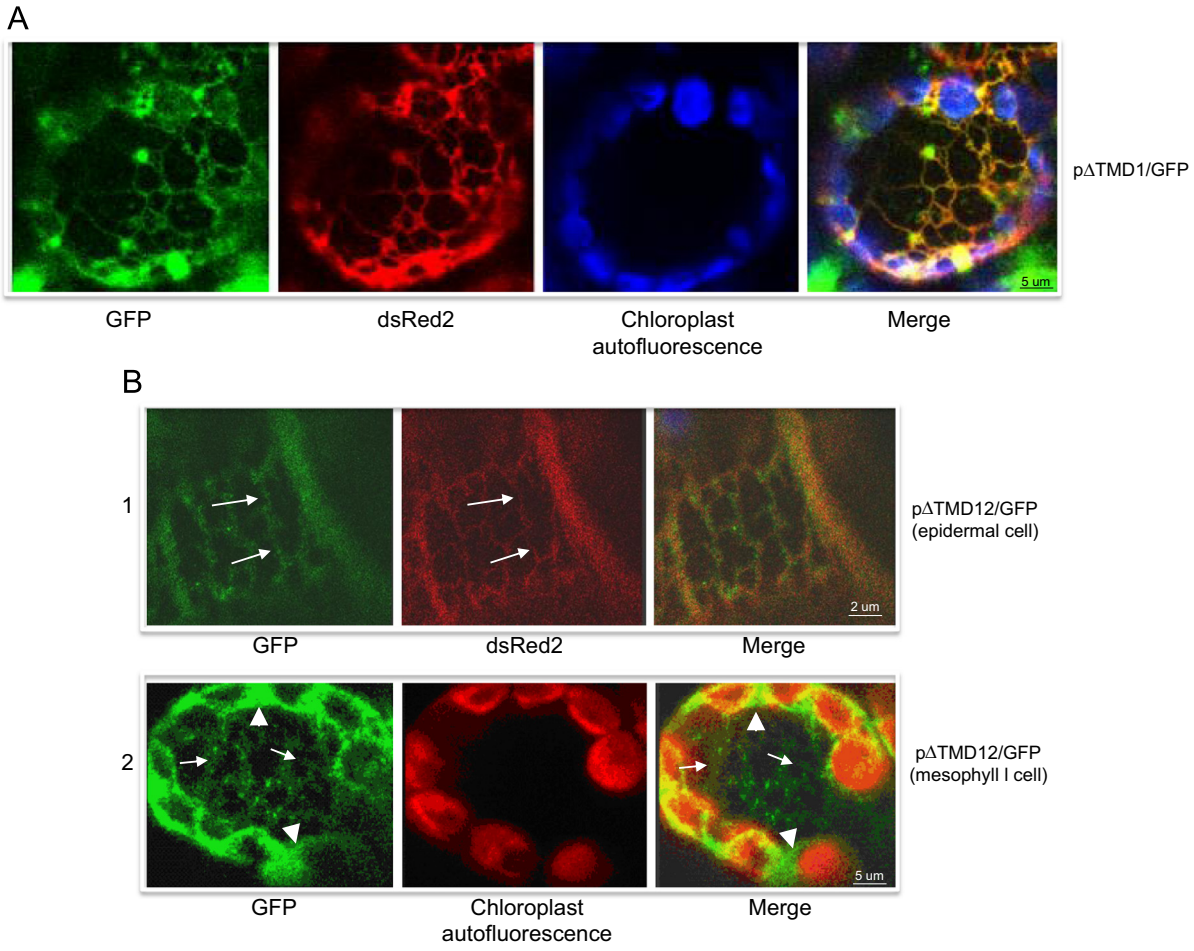

Fig. 5. Confocal microscopy of pΔTMD1/GFP and pΔTMD12/GFP agroinfiltrated leaves. Leaves of *N. benthamiana* were coinfiltrated with pΔTMD1/GFP and pER-dsRed2 (A) or pΔTMD12/GFP and pER-dsRed2 (B) and were examined by confocal microscopy. A) The 4th panel shows that pΔTMD1/GFP colocalizes with pER-dsRed2 in a sharp web like structure in mesophyll cells. The first panel corresponds to GFP fluorescence, the second to dsRed2 and the third to chloroplast autofluorescence (blue). The fourth panel is a digitally merged image of the first three panels. B) ΔTMD12/GFP is loosely associated with the ER as it colocalized with the pER-dsRed2 marker in epidermal cells; however, the signal was often more diffuse than that of the pER-dsRed2 marker (compare GFP with dsRed2 in panel 1). In mesophyll cells (row 2) infiltrated with ΔTMD12/GFP fusion protein also appeared to locate in a diffuse manner with the ER (arrows) and was also present in the cytoplasm surrounding chloroplasts (arrowheads). Note that ER-dsRed2 was not used in B2.

suggest that TMD1 is not required for efficient ER targeting. The "fuzzy" labeling of the ER of pΔTMD12/GFP may represent an unstable association of the encoded protein with the ER as is supported by the presence of green fluorescence in the cytoplasm of the mesophyll cell.

p25/GFP and pΔTMD1/GFP are associated with the membrane component of fractionated cells whereas pΔTMD12/GFP is associated with both the membrane and soluble fractions

Subcellular fractionation studies were conducted to further assess the association of p25/GFP, pΔTMD1/GFP and pΔTMD12/GFP with the ER. Leaves of agroinfiltrated plants were macerated in buffer, filtered and the filtrate was centrifuged at 3000*g* to remove cellular debris. The supernatant (S3) was then subjected to centrifugation at 30,000*g* and the pellet was resuspended in a volume equivalent to the supernatant. The supernatant (S30) contains the soluble fraction and the pellet (P30) contains the membrane fraction including the ER (Zhang and Sanfacon, 2006). Fig. 6A shows that p25/GFP is predominantly associated with the membrane fraction. Similarly, pΔTMD1/GFP with a predicted size of 49 kDa is detected in the P30 fraction (Fig. 6B, lane 12) but not in the S30 fraction (Fig. 6B, lane 9). pΔTMD12/GFP with a predicted size of 41 kDa was found in both the S30 and P30 fractions (Fig. 6B, lanes 10 and 13, respectively). These results are consistent with the notion that p25/GFP and pΔTMD1/GFP target the ER and that pΔTMD12/GFP targets the ER as well as being present in the cytoplasm.

Membrane flotation assays were conducted to confirm the association of p25/GFP, pΔTMD1/GFP and pΔTMD12/GFP with the membrane fraction and to rule out the possibility that association of these proteins with the P30 pellet is due to the presence of highly aggregated protein which is not membrane bound but precipitable due to its large size. In these experiments, proteins associated with the membrane fraction will float near the top of the gradient, whereas aggregated protein which may have pelleted in the P30 fraction will form a pellet on the bottom of the tube. Any contaminating soluble proteins in the P30 fraction will also remain at the bottom of the gradient. Fig. 6C, which is a Western blot containing successive fractions from the gradient, shows that p25/GFP can only be detected at the top of the gradient (see third panel, lanes 2–4,) suggesting that all of p25/GFP is associated with the membrane fraction. Similarly, pΔTMD1/GFP, is found predominantly at the top of the gradient (Fig. 6C, second panel, lanes 3,4) confirming that the loss of predicted TMD1 does not substantially affect the ability of p25 to bind the ER. Conversely, and in agreement with the results of confocal analysis and the cellular fractionation studies, pΔTMD12/GFP is found at both the top and bottom of the gradient (Fig. 6C, top panel). Thus, the

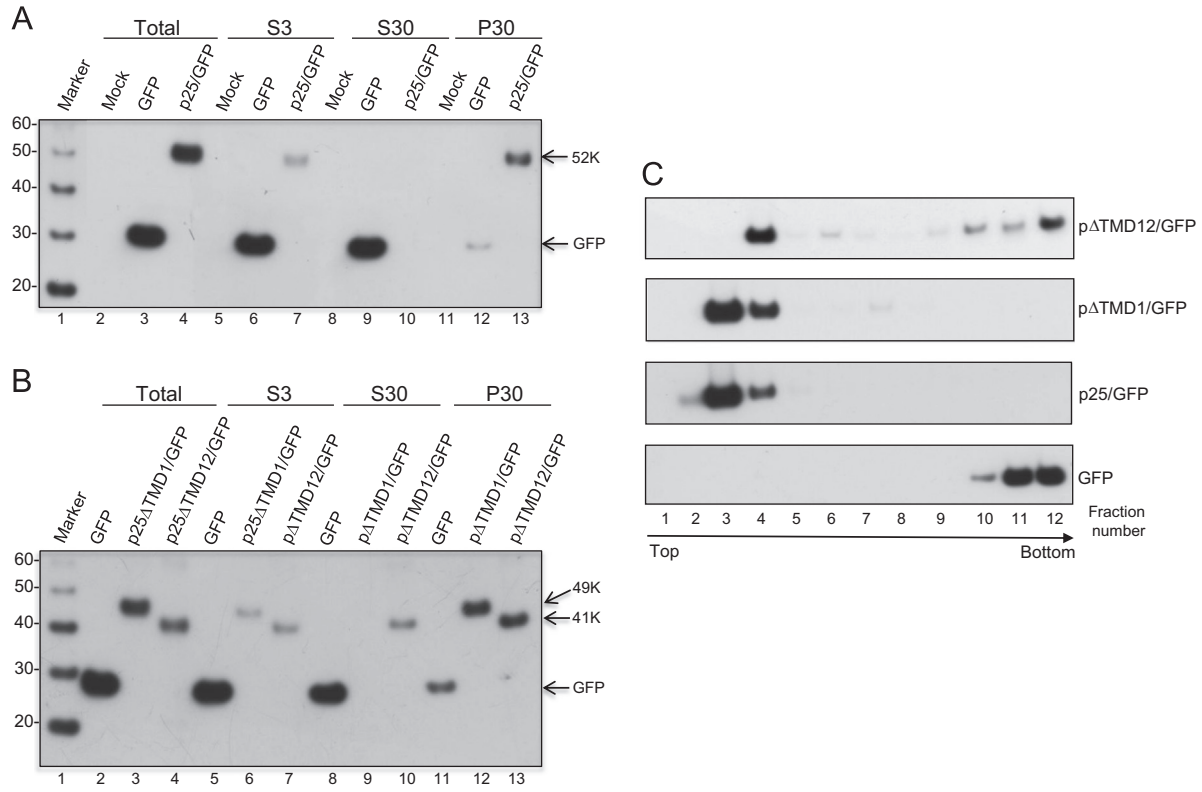

Fig. 6. Subcellular fractionation, membrane flotation assay and immunodetection of p25 and ΔTMD1 and ΔTMD12 deletion mutant GFP fusion proteins. Leaf extracts of plants agroinfiltrated with p25/GFP (A) or with ΔTMD1/GFP and ΔTMD12/GFP (B) were subjected to cellular fractionation via differential centrifugation and the unfractionated (total), 3000*g* supernatant (S3) and the 30,000*g* supernatant (S30) and pellet (P30) were analyzed by SDS PAGE and Western blotting using GFP antiserum. The results show that the full length p25/GFP protein and the ΔTMD1/GFP are predominantly associated with the membrane fraction (panel A, lane 13 and panel B, lane 12, respectively) whereas ΔTMD12/GFP is found in both the soluble and membrane fractions (panel B, lanes 10 and 13). The arrows in A correspond to p25/GFP (52K) and GFP (upper and lower arrows, respectively). In B the arrows correspond to ΔTMD1/GFP (49K), ΔTMD12/GFP (41K) and GFP. (C) *N. benthamiana* plants were agroinfiltrated with p25/GFP and the pΔTMD1/GFP and pΔTMD12/GFP deletion mutants and leaf extracts were subjected to a membrane flotation assay. The results show that full length p25/GFP fusion protein and the ΔTMD1/GFP fusion protein are predominantly associated with the membrane fraction at the top of the gradient consistent with their association with ER. However, the pΔTMD12/GFP mutant is found in both the soluble (bottom) and membrane fraction consistent with the results shown in Fig. 5B, panel 2, where association with the cytoplasm and weak association with the ER are apparent.

predicted TMD2, or possibly both TMD1 and TMD2 play a role in ER attachment.

A third TMD contributes significantly to ER targeting of p25/GFP

As described above we began our search for TMDs in CLSV p25 employing 4 commonly used software packages. However, in view of our observation that removal of TMD1 and TMD2 is not sufficient to largely prevent ER targeting, we used an additional program, SOSUI (Fig. 4) (Hirokawa et al., 1998). This algorithm predicted the presence of a third transmembrane domain that begins at aa 75 and ends at aa 97. A mutant p25/GFP fusion protein construct, pΔTMD123/GFP was produced in which the N-terminal 98 aa of p25 were deleted (Fig. 1). Confocal microscopy of plants co-agroinfiltrated with this construct and pER-dsRed2 showed that GFP and dsRed2 fluorescence did not colocalize (Fig. 7A). Instead, the green fluorescence produced by pΔTMD123/GFP was largely diffuse within the cell. The absence of targeting of pΔTMD123 to the ER suggests that TMD3 plays a prominent role in ER targeting.

To further assess ER targeting of pΔTMD123/GFP, cellular fractionation studies were conducted. Fig. 7C shows that most of ΔTMD123/GFP protein is associated with the S30 fraction indicating that it is mainly not associated with the ER. However, approximately 20% of the signal was observed in the p30 fraction indicating that some interaction with membrane (possibly ER membrane) remained despite undetectable levels of ER targeting as determined by confocal analysis.

Amino acids 1–97 of CLSV p25 are sufficient for ER targeting

The N-terminal 97 aa of CLSV p25 were fused to GFP to determine if the three TMDs are sufficient for ER targeting. This construct ($p25_{aa1-97}$/GFP; see Fig. 1) was co-infiltrated with pER-dsRed2 in *N. benthamiana* plants and then analyzed by confocal microscopy. As shown in Fig. 7B the GFP and dsRed2 signals clearly colocalize indicating that the first 97 aa of CLSV p25 are sufficient for ER targeting. Association with the membrane fraction of cells was confirmed using cellular fractionation and membrane flotation assays (Fig. 7C and D). It can be seen that most of the $p25_{aa1-97}$/GFP protein is associated with the P30 fraction versus the S30 fraction (Fig. 7C, panel 2, compare lanes 5 and 4). In addition, all of the detectable $p25_{aa1-97}$/GFP protein from the p30 fraction floated near the top of the sucrose gradient in a membrane flotation assay (Fig. 7D) further confirming its membrane association.

Cellular fractionation and membrane flotation assays of p25 in CLSV infected leaf tissue

The above described studies are conducted with GFP fusion protein constructs in an agroinfiltration system and therefore may not reflect the actual localization of p25 in CLSV infected plants. Thus CLSV infected leaf tissue was subjected to cellular fractionation and membrane flotation assays followed by Western blot analysis using a p25 specific antibody. It can be seen in Fig. 8 that p25 is predominantly associated with the p30 pellet fraction although approximately 20% of the protein is also detected in

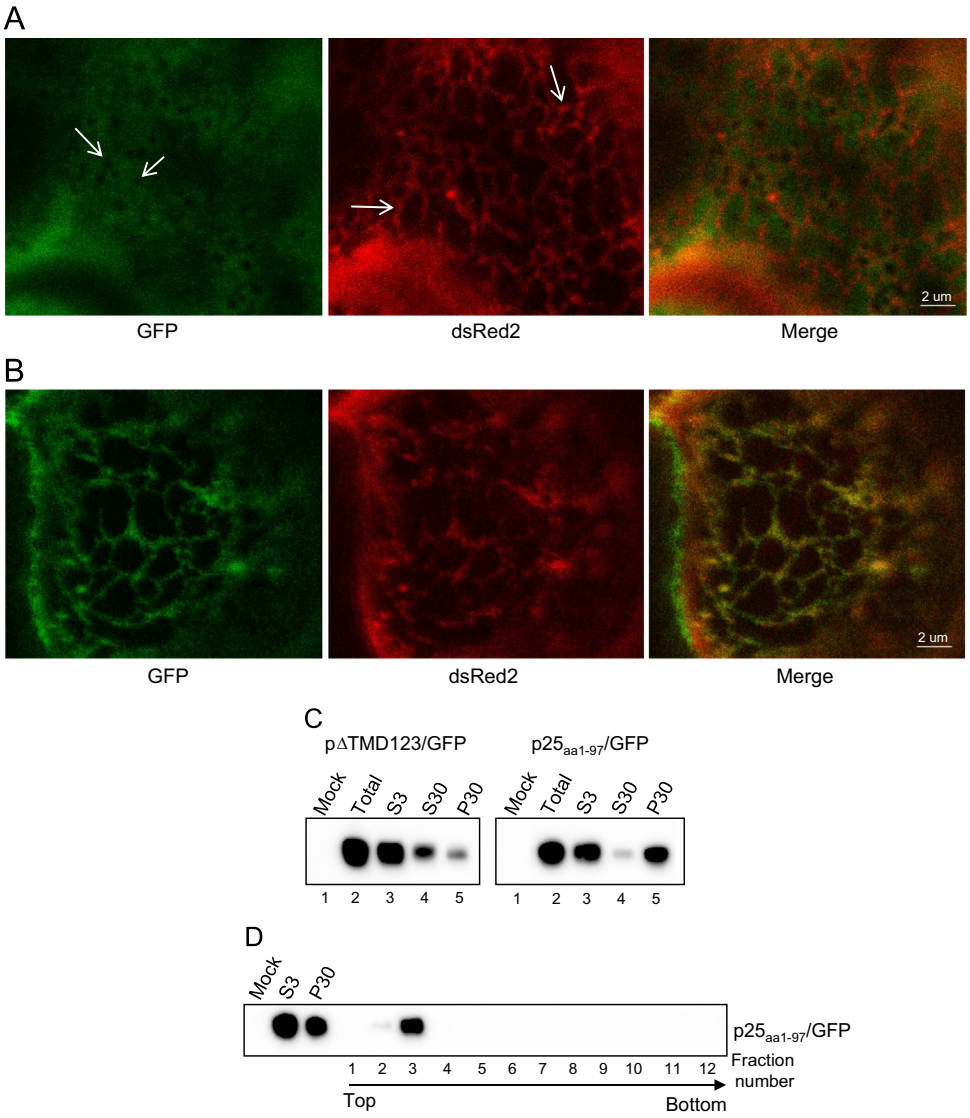

Fig. 7. Confocal microscopy and cellular fractionation analysis of pΔTMD123/GFP and $p25_{aa1-97}$/GFP infiltrated *N. benthamiana* leaves. (A) Leaves were infiltrated with pΔTMD123/GFP and analyzed by confocal microscopy at 4 dpi. GFP fluorescence is cytoplasmic and does not colocalize with the pER-dsRed2 marker as is clearly demonstrated in the merged image in the third panel. The arrows in the first panel point to negative images of mitochondria which result from exclusion of GFP fluorescence in the cytoplasm by the mitochondria. The arrows in the pER-dsRed2 panel point to ER tubules. (B) Leaves were infiltrated with $p25_{aa1-97}$/GFP and analyzed by confocal microscopy at 4 dpi. GFP fluorescence colocalizes with the pER-dsRed2 marker as demonstrated in the merged image in the third panel. (C) Cellular fractionation and membrane flotation assay of pΔTMD123/GFP and $p25_{aa1-97}$/GFP infiltrated leaf tissue. *N. benthamiana* was agroinfiltrated with pΔTMD123/GFP or $p25_{aa1-97}$/GFP and at 4 dpi leaves were macerated and subjected to differential centrifugation as described in the legend to Fig. 6. Equal volumes of the S3, S30 and P30 fractions were subjected to SDS-PAGE and Western blot analysis using a GFP specific antibody. For construct pΔTMD123/GFP it can be seen that the signal in the S30 fraction is more prominent than that in the P30 fraction indicating that pΔTMD123/GFP is mainly in the soluble fraction. For construct $p25_{aa1-97}$/GFP the signal is mainly associated with the P30 membrane fraction. (D) To confirm the association of $p25_{aa1-97}$/GFP with the membrane fraction a membrane flotation assay was conducted utilizing the P30 fraction shown in (C). It can be seen that $p25_{aa1-97}$/GFP is detected exclusively in fractions 2 and 3 near the top of the sucrose gradient indicating that the signal in the p30 fraction indeed represents membrane associated protein rather than precipitated aggregates of p25.

the S30 supernatant. Also, p25 is predominantly detected near the top of the gradient in the membrane flotation study (Fig. 8, lane 3). Together, these results indicate that during infection p25 is associated with the membrane fraction which contains the ER. About 20% of p25 is also apparently present in the soluble fraction. These results are largely in accordance with those conducted using artificial constructs in *Agrobacterium* infiltration assays and therefore assist in validating the results of those studies.

Ultrastructure of CLSV infected plants

CLSV infected *N. benthamiana* plants were subjected to TEM analysis using leaves that were infected for 4 days. A prominent feature of infected plants was the presence of single membrane bound vesicles and or clusters of vesicles sometimes encased in a larger vesicle (Fig. 9A). The smaller vesicles, which were approximately 38–280 nm in diameter could represent the site of replication of CLSV although this requires further confirmation such as determining the presence of the polymerase, p84, and dsRNA. The non-virus containing vesicles did not appear to be classical spherules since close examination did not clearly reveal neck regions open to the cytoplasm. Virus particles were most often present scattered free in the cytoplasm (Fig. 9B, arrowheads).

Encased clusters of vesicles sometimes also contained virus particles as is the case in Fig. 9A. These may therefore represent "virus factories" from proliferated ER as has been found for other viruses including potyviruses, tobamoviruses, nepoviruses, comoviruses, and potexviruses (Laliberte and Sanfacon, 2010).

The nucleus of CLSV infected cells was also found to be modified. Fig. 9B shows that numerous vesicles are present in association with the nucleus, possibly between the nuclear ER and the nuclear membrane. It is possible that the vesicles are derived by invagination and pinching off of the nuclear ER and that this mechanism is also responsible for the "free" vesicles found in the cytoplasm, in this case being derived from cytoplasmic ER.

A comparative study of the ultrastructure of three cucurbit infecting viruses including a East German isolate of CLSV was conducted by Di Franco and Martelli (1987) where it was also shown that CLSV infected cells contained vesicles in the cytoplasm often in groups surrounded by a membrane. In that study, it was also noted that fibrillar material could be observed within the vesicles suggesting that they contained RNA which would be consistent with a role in viral RNA replication. It was also found that vesicles were found within localized dilations of the nuclear envelope. The similar ultrastructure observed in this study and that of Di Franco and Martelli (1987) reinforce the significance of the vesicular structures.

Most, if not all, viruses replicate on specific host membranes and the replicase or auxiliary replicase proteins must have a mechanism for ensuring stable association with the membrane. In the case of CLSV, we show that the p25 auxiliary replicase protein targets the ER and that the N-terminal 97 aa are sufficient for this targeting. Confocal microscopy indicates that p25 may cause elaboration of the ER membrane (including the nuclear ER) possibly resulting in the formation of clusters of vesicles as shown in Fig. 9. In the case of vesicles associated with the nuclear ER it is possible that they are derived via invagination into the lumen of one side of the ER membrane (see below). Vesicles in the cytoplasm are likely similarly derived from cytoplasmic ER.

A model for the positioning of the p25 in the ER membrane is shown in Fig. 10 whereby three N-terminal transmembrane helices traverse one side of the ER membrane. With respect to the ER derived vesicles the C-terminus is likely contained within the vesicle which can be seen as harboring the replicase in the same manner described for spherules and in which the N- and C- termini of the replicase reside in the cytoplasm (den Boon et al., 2010; Laliberte and Sanfacon, 2010). A similar membrane arrangement for the p33–p36 proteins of the tombusviruses, CymRSV, CIRV and TBSV has been described wherein 2 TMDs traverse the membrane and the N- and C- termini are present in the cytoplasm (Navarro et al., 2004; Rajendran and Nagy, 2004; Rubino et al., 2001; Weber-Lotfi et al., 2002). In the case of CLSV, the inside of the vesicle would originate from the cytoplasm. However, this raises the question as to how synthesized RNA could leave the vesicle. It is possible, as in the case of SARS coronavirus double membrane vesicles that these vesicles may actually represent tubules that are connected to the cytoplasm (Knoops et al., 2008). Further research is required to definitively identify the arrangement p25 in vesicles and vesicles as sites of RNA replication.

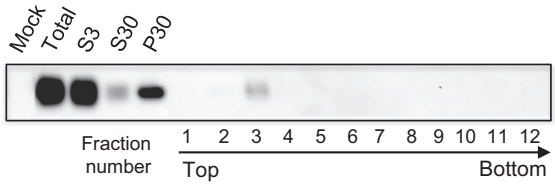

Fig. 8. Fractionation and membrane flotation assay of p25 in CLSV infected leaf tissue. *N. benthamiana* was inoculated with CLSV virions. At 5 dpi leaves were macerated and subjected to differential centrifugation. 10 ml of the 3000*g* supernatant (S3) was centrifuged at 30,000*g* and the pellet (P30) which is enriched for membranes was resuspended in10 ml of buffer (see *Materials and methods*). Equal volumes of the S3, the 30,000*g* supernatant (S30) and P30 fractions were subjected to SDS-PAGE and Western blot analysis using a CLSV p25 specific antibody. It can be seen that the signal in the P30 fraction is more prominent than that in S30 fraction indicating that CLSV p25 is mainly associated with the membrane fraction. To confirm this, a membrane flotation assay was conducted utilizing the P30 fraction. It can be seen that p25 is detected exclusively in fraction 3 near the top of the sucrose gradient indicating that the signal in the p30 fraction indeed represents membrane associated protein rather than precipitated aggregates of p25.

Materials and methods

Plasmid construction

The fusion of the ORF for CLSV p25 with GFP in the binary plasmid vector pBINPLUS (van Engelen et al., 1995) was conducted in two steps. In the first step fusion protein ORFs were cloned into the intermediate vector pBBI525 between the dual 35S promoter and the Nos terminator. In the second step the region from the dual 35S promoter to the Nos terminator was cloned into pBINPLUS. In the first step the construct pBBI525/p25/GFP was made by trimolecular ligation of pBBI525 digested with BamHI, PCR amplified p25 ORF [from the CLSV full-length clone JR3 (Reade et al., 2003)] and the GFP ORF (Xiang et al., 2006). The p25 ORF was amplified using the forward primer NcoI_25K_F and the reverse primer SstII_25K_R and the JR3 plasmid template. The GFP ORF was obtained by SstII and BamHI digestion and purification from a pDRIVE-GFP vector (Table 1). The resulting construct was digested with HindIII and EcoRI and cloned into the corresponding sites of pBINPLUS. The final structure of the p25/GFP construct is shown in Fig. 1.

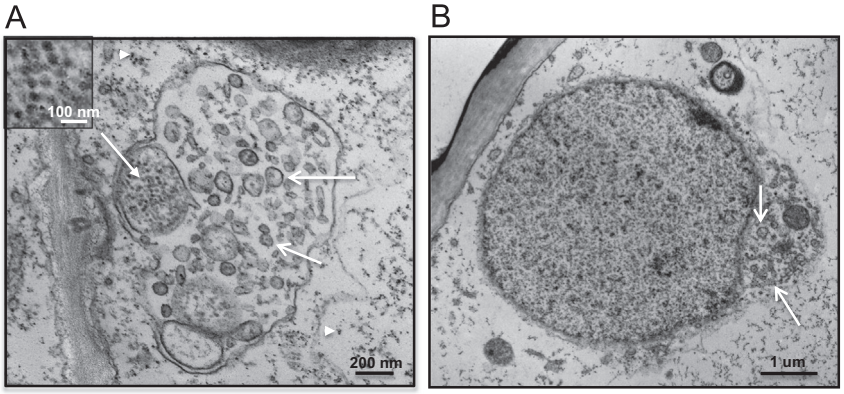

Fig. 9. TEM micrographs of CLSV infected *N. benthamiana* cells. A) A group of membrane bound vesicles which may be used for viral RNA replication. Open arrows point to individual vesicles. Note that a membrane bound group of virus-like particles (closed arrow) (magnified in inset) is found within the group of vesicles suggesting that this structure may represent a virus factory carrying out both replication and encapsidation. Closed arrow heads point to virus particles found in the cytoplasm. B). Nucleus of a cell with an associated group of membrane bound vesicles as in A. This potential site of replication appears to originate from the perinuclear ER of the nucleus and is consistent with confocal microscopy analysis showing GFP labeling of the nuclear membrane (Fig. 2B, panel 2) along with nuclear ER membrane elaborations (Fig. 4, panel 3).

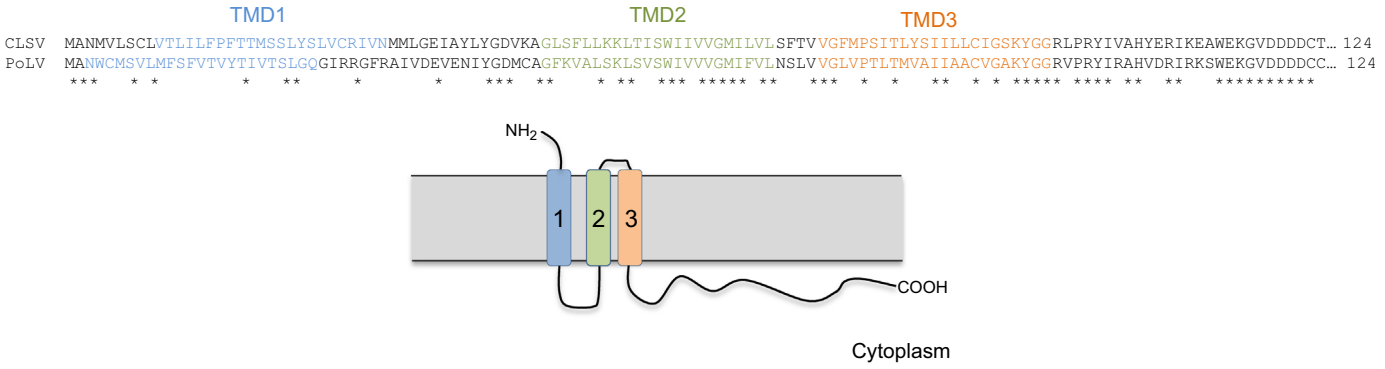

Fig. 10. Comparison and location of TMDs of the p25 proteins of the aureusviruses CLSV and PoLV. A) The N-terminal 124 aa of CLSV and PoLV p25 are aligned with identities shown by the asterisks under the alignment. The three putative TMDs identified using SOSUI are indicated by the colored letters. B) Diagrammatic representation of the orientation of p25 in the ER membrane. The three 23 aa helical TMDs are shown as bars traversing the bilayer membrane (gray). The presumed cytoplasmic side of the membrane is indicated.

Table 1
Oligonucleotides used for construct preparation.

Primer name	Sequence[a]	Purpose
NcoI_25K_F	5′AA**CCATGG***CGAACATGGTCCTAAG* 3′	Forward primer and insertion of NcoI site at 5′end of p25
SstII_25K_R	5′AA**CCGCGG***AAACTCATCGAAGCGTCC* 3′	Reverse primer and insertion of SstII site at 3′ end of p25.
NcoI_ΔTMD1/25K_F	5′AT**CCATGG***TTTGCAGGATTGTGAACATG* 3′	Forward primer for production of pΔTMD1/GFP and insertion of NcoI site at nt 79 of p25 ORF
NcoI_ΔTMD12/25K_F	5′ AT**CCATGG***CAACCTTGTACAGCATTATTTTGC* 3′	Forward primer for production of pΔTMD12/GFP and insertion of NcoI site at nt 244 of p25 ORF
NcoI_ΔTMD123/25K_F	5′*AA***CCATGG***AGCGGATTAAGGAAGCGTG* 3′	Forward primer for production of pΔTMD123/GFP and insertion of NcoI site at nt 323 of p25 ORF
SstII_25K aa 97_R	5′*AA***CCGCGG***CCACGCTTCCTTAATCCGCTC* 3′	Reverse primer for production of p25 aa1-97 and insertion of SstII site at nt 343 of p25 ORF

[a] Letters in bold correspond to restriction enzyme sites used for cloning purposes.

Plasmids pΔTMD1/GFP, pΔTMD12/GFP and pΔTMD123/GFP (Fig. 1) are N-terminal deletion mutants of p25/GFP. pΔTMD1/GFP lacks the N-terminal 78 nucleotides of the p25 ORF, pΔTMD12/GFP lacks the N-terminal 243 nt and, pΔTMD123/GFP lacks the N-terminal 322 nt. These were constructed by bimolecular ligation of pBBI525/GFP SUB (a modified pBBI525 containing GFP) digested with NcoI and SstII and PCR amplified segments corresponding to the 3′terminal 588, 423 and 343 nucleotides, respectively, of the p25 ORF. The pΔTMD1, pΔTMD12 and pΔTMD123 regions were amplified using the primer pairs NcoI_ΔTMD1/25K_F and SstII_25K_R, NcoI_ΔTMD12/25K_F and SstII-25K R and NcoI_ΔTMD123_25KF and SstII_25K_R, respectively (Table 1). The resulting constructs were then digested with HindIII and EcoRI and cloned into the corresponding site of pBINPLUS. $P25_{aa1-97}$/GFP was similarly constructed using a PCR amplified fragment corresponding to aa 1–97 of p25. The forward and reverse primers used to amplify the region corresponding to aa 1–97 were NcoI_25K_F and SstII_25K aa 97_R (Table 1).

Plasmid pER-dsRed2 contains the dsRed2 sequence flanked by an ER targeting N-terminal signal peptide and a C-terminal ER retention signal HDEL (Zhang et al., 2005). Plasmid pGFP was previously described (Rochon et al., 2014).

Agrobacterium-mediated transient expression

All pBINPLUS constructs were used to transform *Agrobacterium tumefaciens* strain GV3101 (Koncz and Schell, 1986) by the freeze and thaw method (Chen et al., 1994). The agroinfiltration procedure was performed as described by others (Guo and Ding, 2002). Transformants were streaked on YEB agar medium (0.1% yeast extract, 0.5% beef extract, 0.5% peptone, 0.5% sucrose, and 2 mM MgSO4, agar) containing the antibiotics kanamycin (100 μg/ml) and rifampicin (80 μg/ml) and incubated at 28 °C for 2 days. A single colony was inoculated into 3 ml YEB liquid medium containing 50 μg/ml kanamycin and 40 μg/ml rifampicin, and grown at 28 °C overnight with vigorous shaking. The 1 ml culture was transferred to 50 ml YEB medium containing the above antibiotics, 10 mM MES (pH 5.6) and 20 μM acetosyringone and incubated overnight at 28 °C. The agrobacteria were centrifuged at 4000*g* for 6 min at 4 °C, and the pellet was resuspended in agroinfiltration buffer (10 mM MES pH 5.6, 10 mM MgCl2, 200 μM acetosyringone) to an OD600 of 1–1.5. The bacteria were then left at room temperature for at least 3 h without shaking. These cultures were used to agroinfiltrate *N. benthamiana* leaves. Simultaneous expression of two different constructs was done by co-infiltration of mixtures of bacterial suspensions. The suspensions were mixed in a 1:1 ratio with each construct having a final OD_{600} of 1–1.5. The TBSV p19 protein was co-expressed in the agroinfiltrated plant cells to suppress induction of gene silencing (Voinnet et al., 2003) thereby allowing optimal expression of the fusion proteins. From two to seven days post-infiltration (dpi) plant leaves were examined daily by confocal microscopy and/or were collected for protein analysis. All experiments were repeated four times, and the results of a representative experiment are shown.

SDS-PAGE and Western blot analysis

Total leaf protein samples were prepared by grinding leaf samples (0.1 g) in liquid nitrogen followed by the addition of 575 μl 1× NuPage® LDS buffer (Invitrogen). Samples were boiled for 10 min and then centrifuged at 10,000*g* for 1 min at RT. Aliquots of protein samples were electrophoresed in Bis-Tris 4–12% mini gels (Invitrogen), and electrotransferred to polyvinylidene difluoride membranes (PVDF, Bio-Rad) according to NuPage® manufacturer's (Invitrogen) protocol. Membranes were blocked with 5% nonfat dry milk solution in 1× Tris-buffered saline (TBS) (50 mM Tris–HCl, pH 8.0, 150 mM NaCl) buffer containing 0.2% Tween 20 (TBS-T). The blot was then incubated with monoclonal GFP antibodies (Amersham) at a 1/5000 dilution in 1× TBS-T for 1 h at room temperature with gentle agitation. Excess antibody was washed from the blot with one

10 min wash followed by two 5 min washes with TBS-T. The blot was then incubated with peroxidase-labelled goat anti-mouse antibody (Sigma-Aldrich) at a 1/10,000 dilution in 1 × TBS-T for 1 h at room temperature with gentle agitation. The blot was washed as described above and reactive protein bands were detected using the Enhanced Chemiluminescence System (ECL;GE Healthcare) according to the manufacturer's instructions and exposed onto Hyperfilm MP (GE Healthcare). Alternatively, the signal was detected using a Bio-Rad GelDoc.

Confocal microscopy

Confocal microscopy was conducted using a Leica SP2-AOBS confocal microscope. GFP and dsRed2 excitation wavelengths were 488 and 543 nm, respectively. GFP fluorescence and dsRed2 fluorescence were captured at emission wavelengths of 507–533 nm and 567–642 nm, respectively. Leaf samples were viewed under a 63 × water immersion objective.

Inoculation of N. benthamiana with CLSV

16C *N. benthamiana* plants were mechanically inoculated with CLSV. 16C plants were kindly provided by Dr. David Baulcombe and CLSV by Dr. Bob Campbell. The CLSV isolate was originally obtained from Dr. I Weber. It is not clear if this is the same isolate used by Franco and Martelli in their ultrastructural investigation of CLSV (Di Franco and Martelli, 1987).

Subcellular fractionation and membrane flotation assays

Subcellular fractionation and membrane flotation assays were conducted as previously described (Sanfacon and Zhang, 2008).

Computer-assisted prediction of putative transmembrane helices

Prediction of transmembrane helices in p25 was performed using the following algorithms: PHDhtm (Rost et al., 1996), Sosui (Hirokawa et al., 1998), Tmpred (Hofmann and Stoffel, 1993), TMHMM (Sonnhammer et al., 1998), HMMTOP (Tusnady and Simon, 1998, 2001).

Transmission electron microscopy

TEM was carried out as previously described using CLSV infected plants at 4 dpi (Rochon et al., 2014).

Acknowledgments

This work was partially supported by NSERC Discovery grant 10R82367. We thank Michael Weis for advice and assistance in confocal and electron microscopy and Joan Chisholm for assistance in membrane fractionation studies.

References

Ahlquist, P., Noueiry, A.O., Lee, W.M., Kushner, D.B., Dye, B.T., 2003. Host factors in positive-strand RNA virus genome replication. J. Virol. 77, 8181–8186.
Brass, V., Bieck, E., Montserret, R., Wölk, B., Hellings, J.A., Blum, H.E., Penin, F., Moradpour, D., 2002. An amino-terminal amphipathic alpha-helix mediates membrane association of thehepatitis C virus nonstructural protein 5A. J Biol Chem. 277, 8130–8139.
Chen, H., Nelson, R.S., Sherwood, J.L., 1994. Enhanced recovery of transformants of Agrobacterium tumefaciens after freeze-thaw transformation and drug selection. Biotechniques 16 (664–668), 670.
den Boon, J.A., Diaz, A., Ahlquist, P., 2010. Cytoplasmic viral replication complexes. Cell Host Microbe 8, 77–85.
den Boon, J.A., Chen, J., Ahlquist, P., 2001. Identification of sequences in Brome mosaic virus replicase protein 1a that mediate association with endoplasmic reticulum membranes. J Virol. 75, 12370–12381.
Di Franco, A., Martelli, G.P., 1987. Comparative ultrastructural investigations on four soil-borne cucurbit viruses. J. Submicrosc. Cytol. 19, 605–613.
dos Reis Figueira, A., Golem, S., Goregaoker, S.P., Culver, J.N., 2002. A nuclear localization signal and a membrane association domain contribute to the cellular localization of the Tobacco mosaic virus 126-kDa replicase protein. Virology 301, 81–89.
Echeverri, A.C., Dasgupta, A., 1995. Amino terminal regions of poliovirus 2C protein mediate membrane binding. Virology 208, 540–553.
Guo, H.S., Ding, S.W., 2002. A viral protein inhibits the long range signaling activity of the gene silencing signal. EMBO J. 21, 398–407.
Hirokawa, T., Boon-Chieng, S., Mitaku, S., 1998. SOSUI: classification and secondary structure prediction system for membrane proteins. Bioinformatics 14, 378–379.
Hofmann, K., Stoffel, W., 1993. TMbase—a database of membrane spanning proteins segments. Biol. Chem. Hoppe-Seyler 374, 166.
Hwang, Y.T., McCartney, A.W., Gidda, S.K., Mullen, R.T., 2008. Localization of the Carnation Italian ringspot virus replication protein p36 to the mitochondrial outer membrane is mediated by an internal targeting signal and the TOM complex. BMC Cell Biol. 9, 54.
Knoops, K., Kikkert, M., Worm, S.H., Zevenhoven-Dobbe, J.C., van der Meer, Y., Koster, A.J., Mommaas, A.M., Snijder, E.J., 2008. SARS-coronavirus replication is supported by a reticulovesicular network of modified endoplasmic reticulum. PLoS Biol. 6, e226.
Koncz, C., Schell, J., 1986. The promoter of Ti-DNA gene controls the tissue specific expression of chimeric genes by a novel type of Agrobacterium binary vector. Mol. Genet. Genomics 204, 383–396.
Kusumanegara, K., Mine, A., Hyodo, K., Kaido, M., Mise, K., Okuno, T., 2012. Identification of domains in p27 auxiliary replicase protein essential for its association with the endoplasmic reticulum membranes in Red clover necrotic mosaic virus. Virology 433, 131–141.
Laliberte, J.F., Sanfacon, H., 2010. Cellular remodeling during plant virus infection. Annu. Rev. Phytopathol. 48, 69–91.
Liu, L., Westler, W.M., den Boon, J.A., Wang, X., Diaz, A., Steinberg, H.A., Ahlquist, P., 2009. An amphipathic alpha-helix controls multiple roles of brome mosaic virus protein 1a in RNA replication complex assembly and function. PLoS Pathog. 5, e1000351.
McCartney, A.W., Greenwood, J.S., Fabian, M.R., White, K.A., Mullen, R.T., 2005. Localization of the tomato bushy stunt virus replication protein p33 reveals a peroxisome-to-endoplasmic reticulum sorting pathway. Plant Cell 17, 3513–3531.
Miller, D.J., Schwartz, M.D., Ahlquist, P., 2001. Flock house virus RNA replicates on outer mitochondrial membranes in Drosophila cells. J. Virol. 75, 11664–11676.
Miller, J.S., Damude, H., Robbins, M.A., Reade, R.D., Rochon, D.M., 1997. Genome structure of cucumber leaf spot virus: sequence analysis suggests it belongs to a distinct species within the Tombusviridae. Virus Res. 52, 51–60.
Miller, S., Krijnse-Locker, J., 2008. Modification of intracellular membrane structures for virus replication. Nat. Rev. Microbiol. 6, 363–374.
Mochizuki, T., Hirai, K., Kanda, A., Ohnishi, J., Ohki, T., Tsuda, S., 2009. Induction of necrosis via mitochondrial targeting of Melon necrotic spot virus replication protein p29 by its second transmembrane domain. Virology 390, 239–249.
Navarro, B., Rubino, L., Russo, M., 2004. Expression of the Cymbidium ringspot virus 33-kilodalton protein in Saccharomyces cerevisiae and molecular dissection of the peroxisomal targeting signal. J. Virol. 78, 4744–4752.
Panavas, T., Hawkins, C.M., Panaviene, Z., Nagy, P.D., 2005. The role of the p33:p33/p92 interaction domain in RNA replication and intracellular localization of p33 and p92 proteins of Cucumber necrosis tombusvirus. Virology 338, 81–95.
Prod'homme, D., Jakubiec, A., Tournier, V., Drugeon, G., Jupin, I., 2003. Targeting of the turnip yellow mosaic virus 66K replication protein to the chloroplast envelope is mediated by the 140K protein. J. Virol. 77, 9124–9135.
Rajendran, K.S., Nagy, P.D., 2004. Interaction between the replicase proteins of Tomato bushy stunt virus in vitro and in vivo. Virology 326, 250–261.
Reade, R., Miller, J., Robbins, M., Xiang, Y., Rochon, D., 2003. Molecular analysis of the cucumber leaf spot virus genome. Virus Res. 91, 171–179.
Rochon, D., Lommel, S., Martelli, G.P., Rubino, L., Russo, M., 2012. Family Tombusviridae. In: King, A.M.Q., Adam, M.J., Carstens, E.B., Lefkowitz, E.J. (Eds.), Virus Taxonomy: Ninth Report of the International Committee on the Taxonomy of Viruses. Elsevier Academic Press, London, pp. 1111–1138.
Rochon, D., Singh, B., Reade, R., Theilmann, J., Ghoshal, K., Alam, S.B., Maghodia, A., 2014. The p33 auxiliary replicase protein of Cucumber necrosis virus targets peroxisomes and infection induces de novo peroxisome formation from the endoplasmic reticulum. Virology 452–453, 133–142.
Rost, B., Casadio, R., Fariselli, P., 1996. Refining neural network predictions for helical transmembrane proteins by dynamic programming. Proc. Int. Conf. Intell. Syst. Mol. Biol. 4, 192–200.
Rubino, L., Weber-Lotfi, F., Dietrich, A., Stussi-Garaud, C., Russo, M., 2001. The open reading frame 1-encoded ('36K') protein of Carnation Italian ringspot virus localizes to mitochondria. J. Gen. Virol. 82, 29–34.
Sanfacon, H., Zhang, G., 2008. Analysis of interactions between viral replicase proteins and plant intracellular membranes. Methods Mol. Biol. 451, 361–375.
Schaad, M.C., Jensen, P.E., Carrington, J.C., 1997. Formation of plant RNA virus replication complexes on membranes: role of an endoplasmic reticulum-targeted viral protein. EMBO J. 16, 4049–4059.

Schmidt-Mende, J., Bieck, E., Hugle, T., Penin, F., Rice, C.M., Blum, H.E., Moradpour, D., 2001. Determinants for membrane association of the hepatitis C virus RNA-dependent RNA polymerase. J Biol Chem. 276, 44052–44063.
Schoelz, J.E., Harries, P.A., Nelson, R.S., 2011. Intracellular transport of plant viruses: finding the door out of the cell. Mol. Plant 4, 813–831.
Schwartz, M., Chen, J., Janda, M., Sullivan, M., den Boon, J., Ahlquist, P., 2002. A positive-strand RNA virus replication complex parallels form and function of retrovirus capsids. Mol. Cell 9, 505–514.
Schwartz, M., Chen, J., Lee, W.M., Janda, M., Ahlquist, P., 2004. Alternate, virus-induced membrane rearrangements support positive-strand RNA virus genome replication. Proc. Natl. Acad. Sci. USA 101, 11263–11268.
Sonnhammer, E.L., von Heijne, G., Krogh, A., 1998. A hidden Markov model for predicting transmembrane helices in protein sequences. Proc. Int. Conf. Intell. Syst. Mol. Biol. 6, 175–182.
Teterina, N.L., Gorbalenya, A.E., Egger, D., Bienz, K., Ehrenfeld, E., 1997. Poliovirus 2C protein determinants of membrane binding and rearrangements in mammalian cells. J. Virol. 71, 8962–8972.
Towner, J.S., Ho, T.V., Semler, B.L., 1996. Determinants of membrane association for poliovirus protein 3AB. J. Biol. Chem. 271, 26810–26818.
Turner, K.A., Sit, T.L., Callaway, A.S., Allen, N.S., Lommel, S.A., 2004. Red clover necrotic mosaic virus replication proteins accumulate at the endoplasmic reticulum. Virology 320, 276–290.
Tusnady, G.E., Simon, I., 1998. Principles governing amino acid composition of integral membrane proteins: application to topology prediction. J. Mol. Biol. 283, 489–506.
Tusnady, G.E., Simon, I., 2001. The HMMTOP transmembrane topology prediction server. Bioinformatics 17, 849–850.
van Engelen, F.A., Molthoff, J.W., Conner, A.J., Nap, J.P., Pereira, A., Stiekema, W.J., 1995. pBINPLUS: an improved plant transformation vector based on pBIN19. Transgenic Res. 4, 288–290.
Van Wynsberghe, P.M., Chen, H.R., Ahlquist, P., 2007. Nodavirus RNA replication protein a induces membrane association of genomic RNA. J. Virol. 81, 4633–4644.
Voinnet, O., Rivas, S., Mestre, P., Baulcombe, D., 2003. An enhanced transient expression system in plants based on suppression of gene silencing by the p19 protein of tomato bushy stunt virus. Plant J. 33, 949–956.
Weber-Lotfi, F., Dietrich, A., Russo, M., Rubino, L., 2002. Mitochondrial targeting and membrane anchoring of a viral replicase in plant and yeast cells. J. Virol. 76, 10485–10496.
Xiang, Y., Kakani, K., Reade, R., Hui, E., Rochon, D., 2006. A 38-amino-acid sequence encompassing the arm domain of the Cucumber necrosis virus coat protein functions as a chloroplast transit peptide in infected plants. J. Virol. 80, 7952–7964.
Zhang, G., Sanfacon, H., 2006. Characterization of membrane association domains within the Tomato ringspot nepovirus X2 protein, an endoplasmic reticulum-targeted polytopic membrane protein. J. Virol. 80, 10847–10857.
Zhang, S.C., Zhang, G., Yang, L., Chisholm, J., Sanfacon, H., 2005. Evidence that insertion of Tomato ringspot nepovirus NTB-VPg protein in endoplasmic reticulum membranes is directed by two domains: a C-terminal transmembrane helix and an N-terminal amphipathic helix. J. Virol. 79, 11752–11765.